

# *Multi-intersection Traffic Light Control with blocking*

**Yanfeng Geng & Christos G. Cassandras**

**Discrete Event Dynamic Systems**  
Theory and Applications

ISSN 0924-6703  
Volume 25  
Combined 1-2

Discrete Event Dyn Syst (2015) 25:7-30  
DOI 10.1007/s10626-013-0176-0

VOLUME 25, NUMBERS 1-2, June 2015  
ISSN 0924-6703

**DISCRETE EVENT  
DYNAMIC SYSTEMS:  
THEORY AND  
APPLICATIONS**

**Editor-in-Chief:**  
*Stephane Lafortune*

 Springer

 Springer

**Your article is protected by copyright and all rights are held exclusively by Springer Science +Business Media New York. This e-offprint is for personal use only and shall not be self-archived in electronic repositories. If you wish to self-archive your article, please use the accepted manuscript version for posting on your own website. You may further deposit the accepted manuscript version in any repository, provided it is only made publicly available 12 months after official publication or later and provided acknowledgement is given to the original source of publication and a link is inserted to the published article on Springer's website. The link must be accompanied by the following text: "The final publication is available at [link.springer.com](http://link.springer.com)".**

## Multi-intersection Traffic Light Control with blocking

Yanfeng Geng · Christos G. Cassandras

Received: 31 January 2013 / Accepted: 13 November 2013 / Published online: 30 November 2013  
© Springer Science+Business Media New York 2013

**Abstract** We address the traffic light control problem for multiple intersections in tandem by viewing it in a stochastic hybrid system setting and developing a Stochastic Flow Model (SFM) for it. Our model includes roads with finite vehicle capacity, which may lead to additional delays due to traffic blocking. Using Infinitesimal Perturbation Analysis (IPA), we derive on-line gradient estimators of an average traffic congestion metric with respect to the controllable green and red cycle lengths. The IPA estimators obtained require counting traffic light switchings and estimating car flow rates only when specific events occur. The estimators are used to iteratively adjust light cycle lengths to improve performance and, in conjunction with a standard gradient-based algorithm, to seek optimal values which adapt to changing traffic conditions. Simulation results are included to illustrate the approach.

**Keywords** Traffic Light Control · Infinitesimal Perturbation Analysis · Hybrid system · Intelligent Transportation System

### Abbreviations

DES	Discrete-Event System
EP	Empty Period
FP	Full Period
G2R	GREEN light to RED light
IPA	Infinitesimal Perturbation Analysis
MDP	Markov Decision Processes
NEP	Non-Empty Period

---

The authors' work is supported in part by NSF under Grants EFRI-0735974 and CNS-1139021, by AFOSR under grant FA9550-12-1-0113, by ONR under grant N00014-09-1-1051, and by ARO under Grant W911NF-11-1-0227.

Y. Geng · C. G. Cassandras (✉)  
Division of Systems Engineering and Center for Information and Systems Engineering,  
Boston University, 15 Saint Mary's Street, Brookline, MA 02446, USA  
e-mail: cgc@bu.edu

Y. Geng  
e-mail: gengyf@bu.edu

NFP	Non-Full Period
R2G	RED light to GREEN light
SCATS	Sydney Coordinated Adaptive Traffic System
SCOOT	Split, Cycle, and Offset Optimization Technique
SFM	Stochastic Flow Model
SHA	Stochastic Hybrid Automaton
TLC	Traffic Light Control

## 1 Introduction

Traffic lights at intersections are the main traffic flow control mechanism in urban road networks. Traffic lights were originally installed in order to guarantee the safe crossing of antagonistic streams of vehicles and pedestrians. With steadily increasing traffic demand, it was soon realized that their presence may also be used to regulate the efficiency of road network operations, hence there must exist an optimal control strategy leading to the minimization of the total time spent by all vehicles in the network (Papageorgiou et al. 2003).

The Traffic Light Control (TLC) problem aims at dynamically controlling the flow of traffic at an intersection through the timing of green/red light cycles with the objective of reducing congestion, hence also the delays incurred by drivers. The general problem involves a set of intersections and traffic lights with the objective of reducing overall congestion over an area covering multiple urban blocks. Control strategies employed for TLC problems are generally classified into two categories: *fixed-cycle strategies* and *traffic-responsive strategies*. Fixed-cycle strategies are derived off-line based on historical demand and turning rate data for each stream; traffic-responsive strategies make use of real-time measurements to calculate and adjust in real-time the best signal settings (Papageorgiou et al. 2003). Recent technological developments involving better, inexpensive sensors and wireless sensor networks have enabled the collection of data (e.g., counting vehicles in a specific road section) which can be used for traffic-responsive strategies. Thus, methodologies that it would not be possible to implement not long ago are now becoming feasible. The approach proposed in this paper to the TLC problem is specifically intended to exploit these recent developments.

*Traffic-responsive strategies* calculate control parameters according to prevailing traffic conditions. They typically respond to changing traffic demand by performing incremental optimization. The most notable of these are SCATS and SCOOT. SCATS (Sydney Coordinated Adaptive Traffic System) (Lowrie 1982) is a real-time control system based on a decentralized architecture. It optimizes the length of cycle times and signal offsets, and allows some phases to be skipped at times. SCOOT (Split, Cycle, and Offset Optimization Technique) (Hunt et al. 1982; Robertson and Bretherton 1991) is a centralized traffic control system, which includes a network model fed with real measurements (instead of historical values) and runs repeatedly in real time to investigate the effect of incremental changes in splits, offsets, and cycle time at individual intersections. If the changes turn out to be beneficial in terms of a performance index, they are submitted to the local signal controllers. Other notable methods under development over the past decade include PROLYN (Henry and Farges 1990), OPAC (Gartner 1983) and RHODES (Sen and Head 1997). These are all traffic-responsive optimization schemes, with various levels of traffic modeling and network-wide optimization capabilities. These strategies do not consider explicitly splits,

offsets, or cycles. Based on prespecified staging, they calculate in real time the optimal values of the next few switching times over a future time horizon.

Numerous algorithms have been proposed to solve the TLC problem. Fuzzy logic is adopted in adaptive traffic signal control to model an expert's knowledge in the situation where development of an exact mathematical model of the phenomenon is very difficult or even impossible (Niittymaki et al. 2002). Pappis and Mamdani (1977) pioneered the implementation of fuzzy logic in a single intersection of two one-way streets without turning traffic. More single-intersection TLC using fuzzy logic can be found in Murat and Gedizlioglu (2005), Trabia et al. (1996) and Wei et al. (2001), where situations such as four-approach streets, left-turning traffic and oversaturated intersections are considered. Nakatsuyama et al. (1984) implemented a fuzzy logic control in two consecutive junctions with one-way movements. Lee et al. presented a fuzzy traffic controller for a set of intersections (Lee et al. 1995), each of which has its own traffic controller.

Using the techniques of Expert Systems (ES), Findler and Stapp (1992) described the control of traffic signals by a network of distributed processors situated at street intersections. Every processor runs an identical expert system and communicates directly with the four adjacent processors. Evolutionary algorithms are also applied in the TLC problem. For example, an improved immunity genetic algorithm was proposed in Liu et al. (2006), a chaos-particle swarm optimization algorithm and catastrophe-particle swarm optimization algorithm were proposed in Dong (2004, 2006), and an ant algorithm was used in Wen and Wu (2005).

Besides artificial intelligence techniques, a game theoretic viewpoint is given in Alvarez and Poznyak (2010), while a hybrid system formulation is presented in Zhao and Chen (2003). It is formulated as a Mixed Integer Linear Programming (MILP) problem in Dujardin et al. (2011), and as an Extended Linear Complementary Problem (ELCP) in DeSchutter (1999). In Porche and Lafortune (1999), the authors proposed an ALLONS-D framework (Adaptive Limited Lookahead Optimization of Network Signals - Decentralized), which is a decentralized method based on the Rolling Horizon (RH) concept.

Since traffic control is fundamentally a problem of sequential decision making, while at the same time it is a task too complex for straightforward computation of optimal solutions, it is well suited to the framework of Markov Decision Processes (MDP) (Yu and Recker 2006) and Reinforcement Learning (RL). Reinforcement learning with full state representation has been proposed in Abdulhai et al. (2003) for a single traffic junction. In Prashanth and Bhatnagar (2011), an RL algorithm with function approximation together with certain graded-feedback policies is proposed. More TLC approaches using RL can be found in Thorpe (1997), Wiering et al. (2004), Bazzan (2009).

Perturbation analysis techniques were first used in Head et al. (1996) and a formal approach using Infinitesimal Perturbation Analysis (IPA) (Cassandras and Lafortune 2008) to solve the TLC problem was presented in Panayiotou et al. (2005) for a single intersection. A Stochastic Fluid Model (SFM) was used to capture the dynamics of the queues formed at an intersection. Estimators of the gradient of a performance measure for traffic congestion with respect to the control parameters were derived based on SFMs. These estimators are evaluated based on observations on the actual Discrete-Event System (DES). The resulting estimates are used with stochastic approximation algorithms to determine the optimal timing. In Geng and Cassandras (2012b), we also studied the TLC problem for a single intersection using a Stochastic Flow Model (SFM) and Infinitesimal Perturbation Analysis (IPA) and in Geng and Cassandras (2012a) we extended our method to multiple intersections in tandem, where we assumed all roads have infinite capacity so that there is no traffic blocking. In this paper, we relax this assumption, so the upstream traffic flow

may be blocked if the downstream road is full. Interestingly, in the case of an intersection upstream from the blocked road section, *all* traffic streams that share this intersection will be blocked, potentially propagating congestion in multiple upstream directions. Therefore, minimizing the probability of blocking becomes much more critical than in strictly serial network configurations.

In our analysis, we adopt a stochastic hybrid system modeling framework (Cassandras and Lygeros 2006), since the problem involves both event-driven dynamics in the switching of traffic lights and time-driven dynamics that capture the flow of vehicles through an intersection. Although one can also view this as a purely Discrete Event System (DES) with the intersection area as a “server” processing “users” (vehicles), the fact that a vehicle does not exclusively occupy this area makes a flow-based viewpoint a more accurate way to model such a process. A SFM as introduced in Cassandras et al. (2002) treats flow models as stochastic processes. In the TLC problem, this is consistent with continuously and randomly varying traffic flows, especially in heavy traffic conditions. With only minor technical assumptions imposed on the properties of such processes, a general IPA theory for stochastic hybrid systems was recently presented in Wardi et al. (2010) and Cassandras et al. (2010) through which one can estimate on-line gradients of certain performance measures with respect to various controllable parameters. These estimates may be incorporated in standard gradient-based algorithms to optimize system parameter settings. IPA estimates become biased when dealing with aspects of queueing systems such as multiple user classes, blocking due to limited resource capacities, and various forms of feedback control. The use of IPA in stochastic hybrid systems, however, circumvents these limitations and yields simple unbiased gradient estimates (under mild technical conditions) of useful metrics (see Yao and Cassandras 2011.) As we will also see, IPA is an event-driven method which scales with the number of observed events over a sample path, not the number of states in the system which is often explosive as its size increases.

The rest of this paper is organized as follows. In Section 2, we formulate the TLC problem for two intersections and construct a SFM. In Section 3, we derive an IPA estimator for a cost function gradient with respect to a controllable parameter vector defined by green and red cycle lengths. Based on this, we also develop a gradient-based algorithm to seek optimal cycle lengths. Simulation-based examples are given in Section 4 and we conclude with Section 5.

## 2 Problem formulation

In this paper, we concentrate on solving the TLC problem for two fully coupled intersections. The same analysis can be readily extended to  $N$  intersections in tandem. As shown in Fig. 1, there are four roads and four traffic lights, with each traffic light controlling the associated incoming traffic flow. The traffic in road 1 of intersection  $I_1$  flows into road 3 of  $I_2$ . For simplicity, we make the following assumptions: (i) Left-turn and right-turn traffic flows are not considered, i.e., traffic lights only control vehicles going straight. (ii) A YELLOW light is combined with a RED light (therefore, the YELLOW light duration is not explicitly controlled).

### 2.1 System dynamics

The system involves a number of stochastic processes which are all defined on a common probability space  $(\Omega, F, P)$ . Each of the four roads is considered as a queue with a random

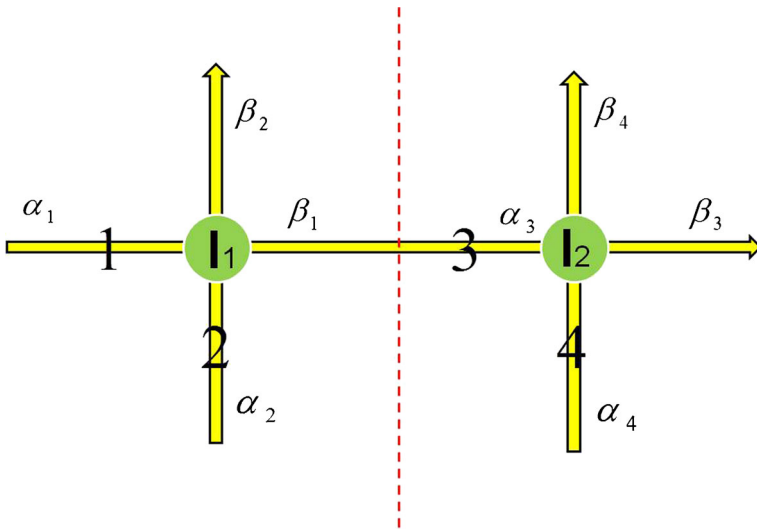


**Fig. 1** Two traffic intersections in tandem

arrival flow process  $\{\alpha_n(t)\}$ ,  $n = 1, \dots, 4$ , where  $\alpha_n(t)$  is the instantaneous vehicle arrival rate at time  $t$ . When the traffic light corresponding to road  $n$  is GREEN, the departure flow process is denoted by  $\{\beta_n(t)\}$ ,  $n = 1, \dots, 4$ . Letting the GREEN light duration in a cycle of queue  $n$  be  $\theta_n$ , then the controllable parameter vector of interest is  $\theta = [\theta_1, \dots, \theta_4]$ . We define a state vector  $x(\theta, t) = [x_1(\theta, t), \dots, x_4(\theta, t)]$  where  $x_n(\theta, t) \in \mathbb{R}^+$  is the content of queue  $n = 1, \dots, 4$ . We use the notation  $x_n(\theta, t)$  to emphasize the dependence of the queue content on  $\theta$ ; however, for notational simplicity, we will write  $x_n(t)$  when no confusion arises. Let  $s_n$  denote the capacity of queue  $n$ ,  $n = 1, \dots, 4$ . Since we do not consider the traffic flow (blocked or not) outside these two intersections, we set  $s_1, s_2$  and  $s_4$  to be infinite and keep only  $s_3$  finite.

We define a “clock” state variable  $z_n(t)$ ,  $n = 1, \dots, 4$ , associated with the GREEN light cycle for queue  $n$  as follows:

$$\begin{aligned} \dot{z}_n(t) &= \begin{cases} 1 & \text{if } 0 < z_n(t) < \theta_n \text{ or } z_{\bar{n}}(t) = \theta_{\bar{n}} \\ 0 & \text{otherwise} \end{cases} \\ z_n(t^+) &= 0 \text{ if } z_n(t) = \theta_n \end{aligned} \tag{1}$$

where  $\bar{n}$  is the index of the road perpendicular to road  $n$  at the same intersection (e.g., if  $n = 1$ , then  $\bar{n} = 2$ ). We set  $z(t) = [z_1(t), \dots, z_4(t)]$ . Thus,  $z_n(t)$  measures the time since the last switch from RED to GREEN of the traffic light for queue  $n$ . It is reset to 0 as soon as the GREEN cycle length  $\theta_n$  is reached and remains at this value while the light is GREEN for queue  $\bar{n}$ ; as soon as that cycle ends, i.e.,  $z_{\bar{n}}(t) = \theta_{\bar{n}}$ , then  $\dot{z}_n(t) = 1$  and the process repeats.

To simplify notation, we define  $G_n(z, \theta) \in \{0, 1\}$  and set  $G_n(z, \theta) = 1$  if the Boolean expression used in (1), i.e.,  $[0 < z_n(t) < \theta_n \text{ or } z_{\bar{n}}(t) = \theta_{\bar{n}}]$ , is true (light is Green) and  $G_n(z, \theta) = 0$  otherwise. We can now write the dynamics of each state variable  $x_n(t)$ ,  $n = 1, \dots, 4$ , as follows:

$$\dot{x}_n(t) = \begin{cases} \alpha_n(t) & \text{if } G_n(z, \theta) = 0 \\ 0 & \text{if } x_n(t) = 0 \text{ and } \alpha_n(t) \leq \beta_n(t) \\ \alpha_n(t) - \beta_n(t) & \text{otherwise} \end{cases} \tag{2}$$

where, for  $n = 2, 3, 4$ :

$$\beta_n(t) = \begin{cases} h_n(t) & \text{if } G_n(z, \theta) = 1 \text{ and } x_n(t) > 0 \\ \alpha_n(t) & \text{if } G_n(z, \theta) = 1 \text{ and } x_n(t) = 0 \\ 0 & \text{otherwise} \end{cases} \quad (3)$$

In (3),  $\{h_n(t)\}$ , defined for all  $n = 1, \dots, 4$ , describes the departure rate process if the road is not empty. This is an external input process depending on vehicle behavior. In general, we should write  $h_n(x_n, t)$ , since this behavior may depend on the traffic conditions in the road section associated with  $x_n(t)$ . In this paper, we will make the simplifying assumption that  $h_n(x_n, t)$  is not dependent on  $x_n(t)$ . It will become clear from our analysis that the IPA estimators obtained can be extended to include such more elaborate traffic dynamics. The definition of  $\beta_1(t)$ , omitted from (3), is more complicated due to the fact that it is also affected by  $x_3(t)$ , especially when  $x_3(t) = s_3$ . Omitting arguments from  $G_n(z, \theta)$ ,  $x_n(t)$ ,  $h_n(t)$ ,  $\alpha_n(t)$ , we have:

$$\beta_1(t) = \begin{cases} h_1 & \text{if } G_1 = 1, x_1 > 0, x_3 < s_3 \\ & \text{or } G_1 = G_3 = 1, x_1 > 0, x_3 = s_3, h_1 < h_3 \\ \alpha_1 & \text{if } G_1 = 1, x_1 = 0, x_3 < s_3 \\ & \text{or } G_1 = G_3 = 1, x_1 = 0, x_3 = s_3, \alpha_1 < h_3 \\ h_3 & \text{if } G_1 = G_3 = 1, x_1 > 0, x_3 = s_3, h_1 \geq h_3 \\ & \text{or } G_1 = G_3 = 1, x_1 = 0, x_3 = s_3, \alpha_1 \geq h_3 \\ 0 & \text{otherwise} \end{cases} \quad (4)$$

In (4), when queue 3 is not full ( $x_3 < s_3$ ), then  $\beta_1(t)$  is the same as (3). However, when queue 3 is full ( $x_3 = s_3$ ) and it has a GREEN light, then  $\beta_1(t)$  is affected by the departure rate of queue 3 and cannot exceed  $h_3(t)$ . If, on the other hand, queue 3 has a RED light, then departures from queue 1 are blocked, i.e.,  $\beta_1(t) = 0$ .

Let us now focus on the dynamics of queues 1,3 since they are directly coupled with each other. Clearly the arrival process of queue 3 is determined by the departure process of queue 1:

$$\alpha_3(t) = \beta_1(t) \quad (5)$$

Combining (2) and (4), we get the dynamics of queue 1 and of queue 3 as follows:

$$\dot{x}_1(t) = \begin{cases} \alpha_1 & \text{if } G_1 = 0 \text{ or } G_1 = 1, x_3 = s_3, G_3 = 0 \\ \alpha_1 - h_1 & \text{if } G_1 = 1, x_1 > 0 \text{ and} \\ & (x_3 < s_3 \text{ or } x_3 = s_3, G_3 = 1, h_1 < h_3) \\ \alpha_1 - h_3 & \text{if } G_1 = G_3 = 1, x_3 = s_3 \text{ and} \\ & (x_1 = 0, \alpha_1 \geq h_3 \text{ or } x_1 > 0, h_1 \geq h_3) \\ 0 & \text{otherwise} \end{cases} \quad (6)$$

$$\dot{x}_3(t) = \begin{cases} h_1 & \text{if } G_3 = 0, G_1 = 1, x_1 > 0, x_3 < s_3 & (7.1) \\ \alpha_1 & \text{if } G_3 = 0, G_1 = 1, x_1 = 0, x_3 < s_3 & (7.2) \\ h_1 - h_3 & \text{if } G_3 = G_1 = 1, x_1 > 0 \text{ and} \\ & (0 < x_3 < s_3 \text{ or } x_3 = s_3, h_1 < h_3) & (7.3) \\ \alpha_1 - h_3 & \text{if } G_3 = G_1 = 1, x_1 = 0 \text{ and} \\ & (0 < x_3 < s_3 \text{ or } x_3 = s_3, \alpha_1 < h_3) & (7.4) \\ -h_3 & \text{if } G_3 = 1, G_1 = 0, x_3 > 0 & (7.5) \\ 0 & \text{otherwise} & (7.6) \end{cases} \quad (7)$$

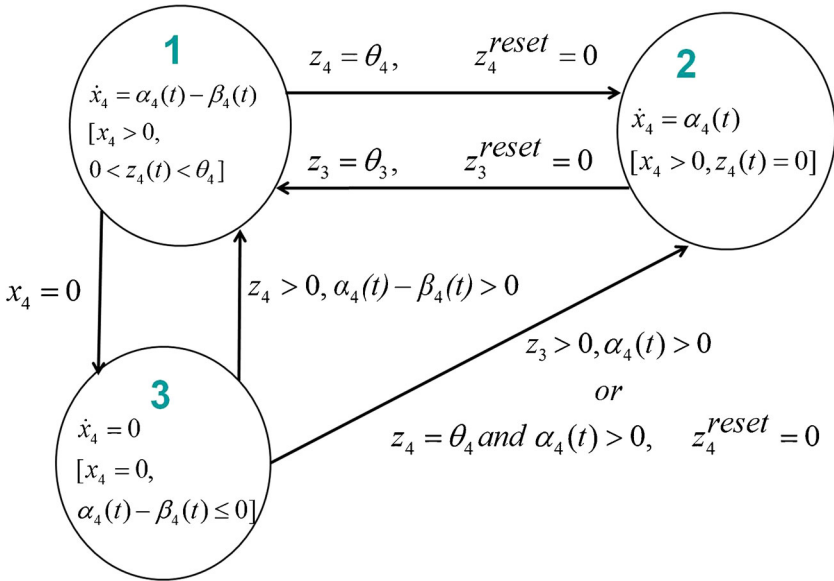


Fig. 2 The Stochastic Hybrid Automaton for queue 4

Finally, taking into account the fact that the whole intersection  $I_1$  is blocked when queue 3 is full, we have:

$$\dot{x}_2(t) = \begin{cases} \alpha_2 & \text{if } G_2 = 0 \text{ or } G_2 = 1, x_3 = s_3 \\ \alpha_2 - h_2 & \text{if } G_2 = 1, x_2 > 0 \text{ and } x_3 < s_3 \\ 0 & \text{otherwise} \end{cases} \quad (8)$$

### 2.2 Stochastic hybrid automaton

The operation of the intersection can be viewed as a hybrid system with the time-driven dynamics described by (1)–(8) and event-driven dynamics, which are dictated by GREEN-RED light switches, by events causing  $x_n(t)$  to switch from positive to zero or vice versa, and by events causing queue 3 to become full or not full.

Using the standard definition of a Stochastic Hybrid Automaton (SHA) (e.g., see Cassandras and Lafortune 2008), we may obtain a SHA model for each queue. We only present the SHA for queue 4 (Fig. 2) which has the simplest dynamics, and queue 3 (Fig. 3) which has the most complicated state transitions. The labeling of the six modes in Fig. 3 corresponds to the six cases with the same labels in (7). The SHA for the other two queues can be similarly obtained. We note that the IPA analysis that follows is based on the formal SFM described by (1)–(8) and does not explicitly involve their SHA counterparts.

A typical sample path of any one of the queue contents (as shown in Fig. 4) consists of intervals over which  $x_n(t) > 0$ , which we call Non-Empty Periods (NEPs), followed by intervals where  $x_n(t) = 0$ , which we call Empty Periods (EPs). Thus, the entire sample path consists of a series of alternating NEPs and EPs. For any NEP, the queue may become full for some intervals, which we call Full Periods (FPs); we call the remaining intervals Non-Full Periods (NFPs). In this model, FPs only arise in the case of queue 3.

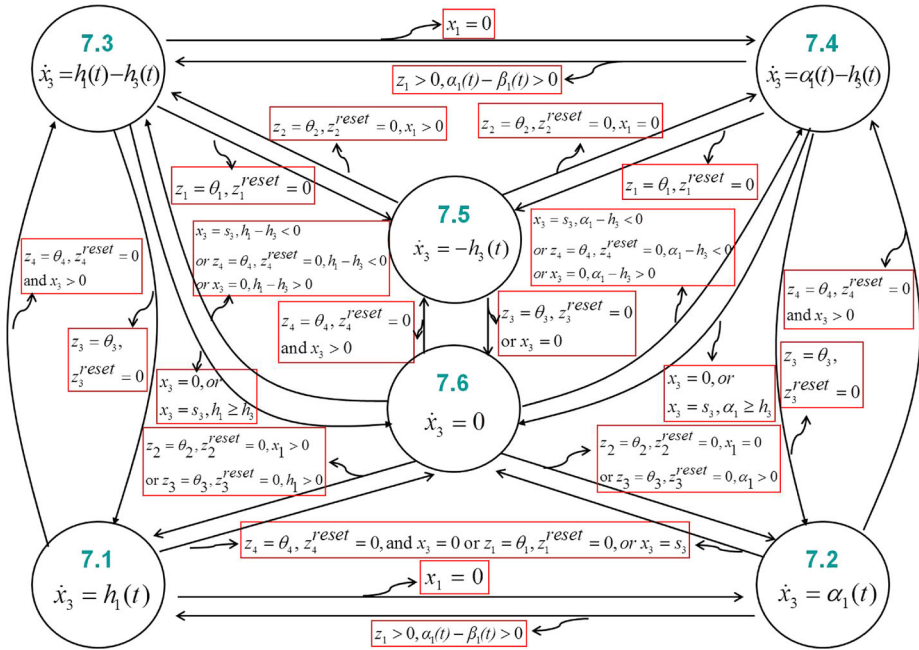


Fig. 3 The Stochastic Hybrid Automaton for queue 3

The event set that affects queue  $n$  is defined as  $\Phi_n = \{e_1, e_2, e_3, e_4, e_5, e_6, e_7\}$  where  $e_1$  is a switch in the sign of  $\alpha_n(t) - \beta_n(t)$  from non-positive to strictly positive;  $e_2$  is a switch in the sign of  $\alpha_n(t) - \beta_n(t)$  from non-negative to strictly negative;  $e_3$  is a switch in the sign of  $\alpha_n(t)$  from 0 to strictly positive;  $e_4$  is the event terminating a NEP (and initiating an EP), i.e., a transition from  $x_i > 0$  to  $x_i = 0$ ;  $e_5$  is the event initiating a FP, i.e., a transition from  $x_i < s_i$  to  $x_i = s_i$ ;  $e_6$  is a light switch from RED to GREEN; and  $e_7$  is a light switch from GREEN to RED. For easier reference, we label  $e_4$  as “ $E_n$ ” for the end of NEP events,  $e_5$  as “ $SF_n$ ” for the start of FP events,  $e_6$  as “ $R2G_n$ ” and  $e_7$  as “ $G2R_n$ ” for the light switching events. The start of a NEP is an event “induced” by either  $e_1$  or  $e_3$  or  $e_7$  which we will refer to as an “ $S_n$ ” event. The end of a FP is an event “induced” by either  $e_2$  or  $e_6$  which we will refer to as an “ $EF_n$ ” event.

The event set associated with queue 3 includes all those events that cause a jump in the value of  $\dot{x}_3(t)$  in (7). As we can see from Fig. 3, every event in  $\Phi_1$  also affects the dynamics of queue 3 and similarly for queue 1. Thus, we have

$$\Phi_3 = \{S_1, E_1, R2G_1, G2R_1, S_3, E_3, R2G_3, G2R_3, SF_3, EF_3\} \tag{9}$$

$$\Phi_1 = \{S_1, E_1, R2G_1, G2R_1, SF_3, EF_3\} \tag{10}$$

Note that there are no  $SF_1$  or  $EF_1$  events since we consider  $s_1$  to be infinite.

Returning to Fig. 4, the  $m$ th NEP in a sample path of queue 3,  $m = 1, 2, \dots$ , is denoted by  $[\xi_{3,m}, \eta_{3,m}]$ , i.e.,  $\xi_{3,m}, \eta_{3,m}$  are the occurrence times of the  $m$ th  $S_3$  and  $E_3$  event respectively at this queue. During the  $m$ th NEP,  $t_{3,m}^j, j = 1, \dots, J_{3,m}$ , denotes the time when an event in  $\Phi_3$  occurs.

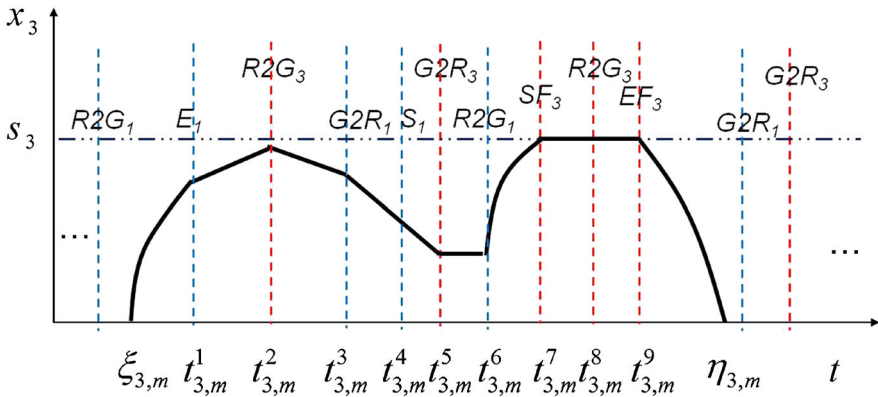


Fig. 4 A typical sample path of traffic light queue 3

### 2.3 Objective function

Our objective is to select  $\theta$  so as to minimize a cost function that measures a weighted mean of the queue lengths over a fixed time interval  $[0, T]$ . In particular, we define the sample function

$$L(\theta; x(0), z(0), T) = \frac{1}{T} \sum_{n=1}^4 \int_0^T w_n x_n(\theta, t) dt \tag{11}$$

where  $w_n$  is a cost weight associated with queue  $n$  and  $x(0), z(0)$  are given initial conditions. It is obvious that since  $x_n(t) = 0$  during EPs of queue  $n$ , we can rewrite (11) in the form

$$L(\theta; x(0), z(0), T) = \frac{1}{T} \sum_{n=1}^4 \sum_{m=1}^{M_n} \int_{\xi_{n,m}(\theta)}^{\eta_{n,m}(\theta)} w_n x_n(\theta, t) dt \tag{12}$$

where  $M_n$  is the total number of NEPs during the sample path of queue  $n$ . For convenience, we also define

$$L_{n,m}(\theta) = \int_{\xi_{n,m}(\theta)}^{\eta_{n,m}(\theta)} x_n(\theta, t) dt \tag{13}$$

to be the cost associated with the  $m$ th NEP of queue  $n$ . We can now define our overall performance metric:

$$J(\theta; x(0), z(0), T) = E[L(\theta; x(0), z(0), T)] \tag{14}$$

Since we do not impose any limitations on the processes  $\{\alpha_n(t)\}$  and  $\{\beta_n(t)\}$ , it is infeasible to obtain a closed-form expression of  $J(\theta; x(0), z(0), T)$ . The only assumption we make is that  $\alpha_n(t), \beta_n(t)$  are piecewise continuous w.p. 1. The value of IPA as developed for general stochastic hybrid systems in Cassandras et al. (2010) lies in providing an estimate of the performance metric gradient  $\nabla J(\theta)$ , by evaluating the sample gradient  $\nabla L(\theta)$ . These estimates are unbiased under mild technical conditions as discussed in Cassandras et al. (2010). Moreover, an important property of IPA estimates is that they are often independent of the unknown processes  $\{\alpha_n(t)\}$  and  $\{\beta_n(t)\}$  or they depend on values of  $\alpha_n(t)$  or  $\beta_n(t)$  at *specific event times only*. One can then use this information to either improve performance

or, under appropriate conditions, solve an optimization problem and determine an optimal  $\theta^*$  through an iterative scheme:

$$\theta_{i,k+1} = \theta_{i,k} - \gamma_k H_{i,k}(\theta_k, x(0), T, \omega_k), k = 0, 1, \dots \tag{15}$$

where  $H_{i,k}(\theta_k, x(0), T, \omega_k)$  is an estimate of  $dJ/d\theta_i$  (in our case, the IPA derivative estimate) based on the information obtained from the sample path denoted by  $\omega_k$ , and  $\gamma_k$  is the stepsize at the  $k$ th iteration. Next we will focus on obtaining  $dL/d\theta_i, i = 1, \dots, 4$ . We may then also obtain  $\theta^*$  through (15), provided that the random processes  $\{\alpha_n(t)\}$  and  $\{\beta_n(t)\}$  are stationary over  $[0, T]$ . We will assume that the derivatives  $dL/d\theta_i$ , exist for all  $\theta_i \in \mathbb{R}^+$  w.p. 1.

Finally, it is worth pointing out that the choice of cost function in (11) does not restrict our analysis. This is because the IPA estimators we derive are for state and event time sensitivities, therefore, any cost or performance criterion expressed in terms of these variables can be accommodated in this framework subject only to some technical conditions (see Cassandras and Lafortune 2010).

### 3 Infinitesimal perturbation analysis

Consider a sample path of the system over  $[0, T]$  and let  $\tau_k(\theta)$  denote the occurrence time of the  $k$ th event (of any type), where we stress its dependence on  $\theta$ . To simplify notation, we define the derivatives of the states  $x_n(t, \theta)$  and event times  $\tau_k(\theta)$  with respect to  $\theta_i, i = 1, \dots, 4$ , as follows:

$$x'_{n,i}(t) \equiv \frac{\partial x_n(\theta, t)}{\partial \theta_i}, \tau'_{k,i} \equiv \frac{\partial \tau_k(\theta)}{\partial \theta_i} \tag{16}$$

Taking derivatives with respect to  $\theta_i$  in (12), we obtain

$$\begin{aligned} \frac{dL(\theta)}{d\theta_i} = & \frac{1}{T} \sum_{n=1}^4 \sum_{m=1}^{M_n} \left[ \int_{\xi_{n,m}(\theta)}^{\eta_{n,m}(\theta)} w_n x'_{n,i}(t) dt \right. \\ & \left. + w_n x_n(\eta_{n,m}) \frac{\partial \eta_{n,m}}{\partial \theta_i} - w_n x_n(\xi_{n,m}) \frac{\partial \xi_{n,m}}{\partial \theta_i} \right] \end{aligned}$$

Since, at the start and end of a NEP  $x_n(\xi_{n,m}) = x_n(\eta_{n,m}) = 0$ , this reduces to

$$\begin{aligned} \frac{dL(\theta)}{d\theta_i} = & \frac{1}{T} \sum_{n=1}^4 \sum_{m=1}^{M_n} \int_{\xi_{n,m}}^{\eta_{n,m}} w_n x'_{n,i}(t) dt \\ \equiv & \frac{1}{T} \sum_{n=1}^4 \sum_{m=1}^{M_n} w_n \frac{dL_{n,m}(\theta)}{d\theta_i} \end{aligned} \tag{17}$$

where the last equality follows from the definition (13).

#### 3.1 IPA review

Before proceeding, we provide a brief review of the IPA framework for general stochastic hybrid systems as presented in Cassandras et al. (2010). Let  $\{\tau_k(\theta)\}, k = 1, \dots, K$ , denote the occurrence times of all events in the state trajectory. For convenience, we set  $\tau_0 = 0$  and  $\tau_{K+1} = T$ . Over an interval  $[\tau_k(\theta), \tau_{k+1}(\theta))$ , the system is at some mode during which the time-driven state satisfies  $\dot{x} = f_k(x, \theta, t)$ . An event at  $\tau_k$  is classified as (i) *Exogenous* if

it causes a discrete state transition independent of  $\theta$  and satisfies  $\frac{d\tau_k}{d\theta} = 0$ ; (ii) *Endogenous*, if there exists a continuously differentiable function  $g_k : \mathbb{R}^n \times \Theta \rightarrow \mathbb{R}$  such that  $\tau_k = \min\{t > \tau_{k-1} : g_k(x(\theta, t), \theta) = 0\}$ ; and (iii) *Induced* if it is triggered by the occurrence of another event at time  $\tau_m \leq \tau_k$ . IPA specifies how changes in  $\theta$  influence the state  $x(\theta, t)$  and the event times  $\tau_k(\theta)$  and, ultimately, how they influence interesting performance metrics which are generally expressed in terms of these variables.

Given  $\theta = [\theta_1, \dots, \theta_r]^T$ , we use the Jacobian matrix notation:  $x'(t) \equiv \frac{\partial x(\theta, t)}{\partial \theta}$ ,  $\tau'_k \equiv \frac{\partial \tau_k(\theta)}{\partial \theta}$ ,  $k = 1, \dots, K$ , for all state and event time derivatives. It is shown in Cassandras et al. (2010) that  $x'(t)$  satisfies:

$$\frac{d}{dt}x'(t) = \frac{\partial f_k(t)}{\partial x}x'(t) + \frac{\partial f_k(t)}{\partial \theta} \tag{18}$$

for  $t \in [\tau_k, \tau_{k+1})$  with boundary condition:

$$x'(\tau_k^+) = x'(\tau_k^-) + [f_{k-1}(\tau_k^-) - f_k(\tau_k^+)] \tau'_k \tag{19}$$

for  $k = 0, \dots, K$ . In addition, in (19), the gradient vector for each  $\tau_k$  is  $\tau'_k = 0$  if the event at  $\tau_k$  is exogenous and

$$\tau'_k = - \left[ \frac{\partial g_k}{\partial x} f_k(\tau_k^-) \right]^{-1} \left( \frac{\partial g_k}{\partial \theta} + \frac{\partial g_k}{\partial x} x'(\tau_k^-) \right) \tag{20}$$

if the event at  $\tau_k$  is endogenous (i.e.,  $g_k(x(\theta, \tau_k), \theta) = 0$ ) and defined as long as  $\frac{\partial g_k}{\partial x} f_k(\tau_k^-) \neq 0$ .

In our problem, according to (2), (6) and (7), we have  $\frac{\partial f_{n,k}}{\partial x_n} = \frac{\partial f_{n,k}}{\partial \theta_i} = 0$  between two events, and we get  $\frac{d}{dt}x'_{n,i}(t) = 0$  in (18). Therefore,  $x'_{n,i}(t)$  remains constant over all  $t \in [\tau_k, \tau_{k+1})$ :

$$x'_{n,i}(t) = x'_{n,i}(\tau_k^+), \quad t \in [\tau_k, \tau_{k+1}) \tag{21}$$

### 3.2 State and event time derivatives

In what follows, we focus on each event type at queue 3, identified in the set  $\Phi_3$  in (9), and derive the corresponding event time derivatives. Based on these, we can then also derive  $x'_{3,i}(t)$  and hence  $dL_{3,m}/d\theta_i$ . This analysis also covers all cases for queues 1, 2 and 4, which have simpler dynamics. Thus, we will not consider them separately (original derivations of these simpler cases were first given in Geng and Cassandras 2012b). However, due to the blocking effects considered in this paper, there are some cases where  $x'_{1,i}(t)$  and  $x'_{2,i}(t)$  are different from the original analysis in Geng and Cassandras (2012b). When these cases arise based on the dynamics in (6) and (8), we will also derive  $x'_{1,i}(t)$  and  $x'_{2,i}(t)$ .

- (1) **Event  $E_1$  ends a NEP of queue 1.** This is an endogenous event that occurs when  $g_k(x(\theta, t), \theta) = x_1(\theta, t) = 0$ . Using (20) and observing that  $f_{1,k-1}(\tau_k^-) = \alpha_1(\tau_k^-) - h_1(\tau_k^-)$  from (2), we get

$$\tau'_{k,i} = \frac{-x'_{1,i}(\tau_k^-)}{\alpha_1(\tau_k^-) - h_1(\tau_k^-)}$$

Looking at (7), we have either  $f_{3,k-1}(\tau_k^-) = h_1(\tau_k^-) - h_3(\tau_k^+)$  and  $f_{3,k}(\tau_k^+) = \alpha_1(\tau_k^-) - h_3(\tau_k^+)$  when  $G_3(z, \theta) = 1$ , or  $f_{3,k-1}(\tau_k^-) = h_1(\tau_k^-)$  and

$f_{3,k}(\tau_k^+) = \alpha_1(\tau_k^-)$  when  $G_3(z, \theta) = 0$ . In both cases,  $f_{3,k-1}(\tau_k^-) - f_{3,k}(\tau_k^+) = h_1(\tau_k^-) - \alpha_1(\tau_k^-)$ . Using these values in (19) along with  $\tau'_{k,i}$  above we get

$$x'_{3,i}(\tau_k^+) = x'_{3,i}(\tau_k^-) + x'_{1,i}(\tau_k^-), \quad i = 1, \dots, 4 \tag{22}$$

As we can see,  $x'_{3,i}(\tau_k^+)$  explicitly depends on  $x'_{1,i}(\tau_k^-)$ . This indicates that a ‘‘perturbation’’ in the content of queue 1 ‘‘propagates’’ downstream to queue 3 whenever an EP at queue 1 takes place.

- (2) **Event  $E_3$  ends a NEP of queue 3.** This is an endogenous event occurring when  $x_3(\theta, t) = 0$ . Using (20), we get  $\tau'_{k,i} = \frac{-x'_{3,i}(\tau_k^-)}{f_{3,k-1}(\tau_k^-)}$ . According to (7), we have  $f_{3,k}(\tau_k^+) = 0$ . Using these values in (19) along with  $\tau'_{k,i}$  above we get

$$x'_{3,i}(\tau_k^+) = x'_{3,i}(\tau_k^-) - f_{3,k-1}(\tau_k^-) \frac{x'_{3,i}(\tau_k^-)}{f_{3,k-1}(\tau_k^-)} = 0, \quad i = 1, \dots, 4 \tag{23}$$

This indicates that these state derivatives at queue 3 are always reset to 0 upon ending a NEP of queue 3.

- (3) **Event  $G2R_1$ .** This is an endogenous event that occurs when  $z_1(\tau_k) = \theta_1$ . The following lemma allows us to determine  $\tau'_{k,i}$ .

**Lemma 1** *Let  $\zeta_{1,k}$  be the total number of  $G2R_1$  events that have occurred before or at  $\tau_k$ , and  $\rho_{1,k}$  be the total number of  $R2G_1$  events that have occurred before or at  $\tau_k$ . Then,  $\tau'_{k,1} = \zeta_{1,k}$ ,  $\tau'_{k,2} = \rho_{1,k}$ ,  $\tau'_{k,3} = 0$  and  $\tau'_{k,4} = 0$*

*Proof* Since the event at  $\tau_k$  is the  $\zeta_{1,k}$ th occurrence of a  $G2R_1$  event, we can write  $\tau_k = \zeta_{1,k}\theta_1 + \rho_{1,k}\theta_2 - K(z(0))$  where  $K(z(0))$  is a constant (independent of  $\theta_1$ ) dependent on the initial conditions  $z_1(0)$ ,  $z_2(0)$ . It immediately follows that  $\tau'_{k,1} = \zeta_{1,k}$ . A similar argument yields  $\tau'_{k,2} = \rho_{1,k}$  and  $\tau'_{k,3} = \tau'_{k,4} = 0$ . □

According to (7), we have either  $f_{3,k-1}(\tau_k^-) - f_{3,k}(\tau_k^+) = h_1(\tau_k^-)$  (from (7.1)-(7.6), or (7.3)-(7.5)), or  $f_{3,k-1}(\tau_k^-) - f_{3,k}(\tau_k^+) = \alpha_1(\tau_k^-)$  (from (7.2)-(7.6), or (7.4)-(7.5)). Using (3), we can combine these two situations so that  $f_{3,k-1}(\tau_k^-) - f_{3,k}(\tau_k^+) = \beta_1(\tau_k^-)$ . It then follows from (19) that

$$x'_{3,i}(\tau_k^+) = \begin{cases} x'_{3,i}(\tau_k^-) + \beta_1(\tau_k^-)\zeta_{1,k} & i = 1 \\ x'_{3,i}(\tau_k^-) + \beta_1(\tau_k^-)\rho_{1,k} & i = 2 \\ x'_{3,i}(\tau_k^-) & i = 3, 4 \end{cases} \tag{24}$$

It is worth pointing out that if  $G2R_1$  occurs while  $x_3 = s_3$ , the value of  $\dot{x}_2(t)$  in (8) does not change due to blocking, i.e.,  $f_{2,k-1}(\tau_k^-) = f_{2,k}(\tau_k^+) = \alpha_2(\tau_k)$ . Thus, using (19) we get  $x'_{2,i}(\tau_k^+) = x'_{2,i}(\tau_k^-)$  for all  $i = 1, \dots, 4$ .

- (4) **Event  $G2R_3$ .** This is an endogenous event that occurs when  $z_3(\tau_k) = \theta_3$ .  $\tau'_{k,i}$  is determined by the following lemma whose proof is similar to that of Lemma 1.

**Lemma 2** *Let  $\zeta_{3,k}$  be the total number of  $G2R_3$  events that have occurred before or at  $\tau_k$ , and  $\rho_{3,k}$  be the total number of  $R2G_3$  events that have occurred before or at  $\tau_k$ . Then,  $\tau'_{k,3} = \zeta_{3,k}$ ,  $\tau'_{k,4} = \rho_{3,k}$ ,  $\tau'_{k,1} = 0$  and  $\tau'_{k,2} = 0$*

From (7), if  $x_3(\tau_k^-) > 0$ , we have  $f_{3,k-1}(\tau_k^-) - f_{3,k}(\tau_k^+) = -h_3(\tau_k^-)$  (from (7.3)-(7.1), or (7.4)-(7.2), or (7.5)-(7.6)). According to (19),

$$x'_{3,i}(\tau_k^+) = \begin{cases} x'_{3,i}(\tau_k^-) & i = 1, 2 \\ x'_{3,i}(\tau_k^-) - h_3(\tau_k^-)\xi_{3,k} & i = 3 \\ x'_{3,i}(\tau_k^-) - h_3(\tau_k^-)\rho_{3,k} & i = 4 \end{cases} \tag{25}$$

If  $x_3(\tau_k^-) = 0$ ,  $f_{3,k-1}(\tau_k^-) - f_{3,k}(\tau_k^+) = -\beta_1(\tau_k^+)$  (from (7.6)-(7.1), or (7.6)-(7.2)). Then,

$$x'_{3,i}(\tau_k^+) = \begin{cases} x'_{3,i}(\tau_k^-) & i = 1, 2 \\ x'_{3,i}(\tau_k^-) - \beta_1(\tau_k^+)\xi_{3,k} & i = 3 \\ x'_{3,i}(\tau_k^-) - \beta_1(\tau_k^+)\rho_{3,k} & i = 4 \end{cases} \tag{26}$$

In this case, we see that the value of  $x'_{3,i}(\tau_k^+)$  depends on whether the  $G2R_3$  event occurs when there is any traffic waiting at the light or not.

- (5) **Event  $R2G_1$ .** This is similar to case (3) and we obtain  $x'_{3,i}(\tau_k^-)$  without giving details:

$$x'_{3,i}(\tau_k^+) = \begin{cases} x'_{3,i}(\tau_k^-) - \beta_1(\tau_k^+)\xi_{1,k} & i = 1 \\ x'_{3,i}(\tau_k^-) - \beta_1(\tau_k^+)\rho_{1,k} & i = 2 \\ x'_{3,i}(\tau_k^-) & i = 3, 4 \end{cases} \tag{27}$$

Similar to case (3), if  $R2G_1$  occurs while  $x_3 = s_3$ , we also have  $f_{2,k-1}(\tau_k^-) = f_{2,k}(\tau_k^+) = \alpha_2(\tau_k)$ . Hence, using (19),  $x'_{2,i}(\tau_k^+) = x'_{2,i}(\tau_k^-)$  for all  $i = 1, \dots, 4$ .

- (6) **Event  $R2G_3$ .** This is similar to case (4) and we obtain  $x'_{3,i}(\tau_k^-)$  without giving details:

$$x'_{3,i}(\tau_k^+) = \begin{cases} x'_{3,i}(\tau_k^-) & i = 1, 2 \\ x'_{3,i}(\tau_k^-) + h_3(\tau_k^+)\xi_{3,k} & i = 3 \\ x'_{3,i}(\tau_k^-) + h_3(\tau_k^+)\rho_{3,k} & i = 4 \end{cases} \tag{28}$$

- (7) **Event  $S_1$  starts a NEP of queue 1** As already mentioned, this is an event induced by  $e_5, e_2$ , or  $e_1$  (see Fig. 5). Consequently, there are three possible cases to consider as follows.

**Case (7a)** *A NEP of queue 1 starts right after a  $G2R_1$  event.* This is an endogenous event and was analyzed in Case (3). Since  $x_1(\tau_k^-) = 0$ , we have  $\beta_1(\tau_k^-) = \alpha_1(\tau_k^-)$  in (3) and we get in (24):

$$x'_{3,i}(\tau_k^+) = \begin{cases} x'_{3,i}(\tau_k^-) + \alpha_1(\tau_k^-)\xi_{1,k} & i = 1 \\ x'_{3,i}(\tau_k^-) + \alpha_1(\tau_k^-)\rho_{1,k} & i = 2 \\ x'_{3,i}(\tau_k^-) & i = 3, 4 \end{cases} \tag{29}$$

**Case (7b)** *A NEP of queue 1 starts while  $z_1(\tau_k) = 0, z_2(\tau_k) > 0$ .* This is an exogenous event occurring during a RED cycle for queue 1 and is due to a change in  $\alpha_1(\tau_k)$  from zero to a strictly positive value. Therefore,  $\tau'_{k,i} = 0$ . We then have from (19):

$$x'_{3,i}(\tau_k^+) = x'_{3,i}(\tau_k^-), \quad i = 1, 2, 3, 4 \tag{30}$$

**Case (7c)** *A NEP of queue 1 starts while  $z_2(\tau_k) = 0, z_1(\tau_k) > 0$ .* This is an exogenous event occurring during a GREEN cycle for queue 1 due to a

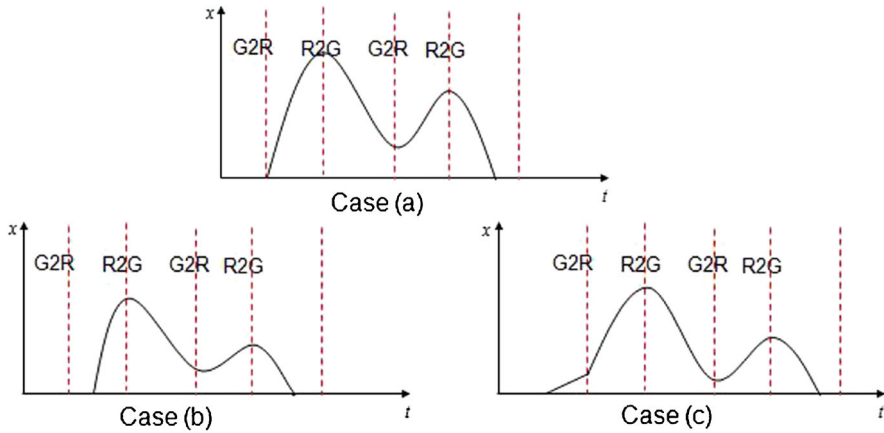


**Fig. 5** Three ways for starting a NEP

change in  $\alpha_1(\tau_k)$  or  $\beta_1(\tau_k)$  that results in  $\alpha_1(\tau_k) - \beta_1(\tau_k)$  switching from a non-positive to a strictly positive value. The analysis is exactly the same as Case (7b) above and (30) applies.

- (8) **Event  $S_3$  starts a NEP of queue 3.** This is similar to Case (7), and there are also three possible cases.

**Case (8a)** A NEP of queue 3 starts right after a  $G2R_3$  event. This is an endogenous event and was analyzed in Case (4). In particular, since  $x_3(\tau_k^-) = 0$ , (26) applies. Suppose that this is the  $m$ th NEP, i.e.,  $\tau_k = \xi_{3,m}$ . We have already shown in (23) that  $x'_{3,i}(\eta_{n,m-1}^+) = 0$ . In addition, we have  $x_3(t) = 0$  over the interval  $[\eta_{3,m-1}, \xi_{3,m})$ , thus  $x'_{3,i}(t) = 0$  for all  $t \in [\eta_{3,m-1}, \xi_{3,m})$  and we get  $x'_{3,i}(\tau_k^-) = x'_{3,i}(\xi_k^-) = 0$ . Therefore,  $x'_{3,i}(\tau_k^+)$  in (26) becomes

$$x'_{3,i}(\tau_k^+) = \begin{cases} 0 & i = 1, 2 \\ -\beta_1(\tau_k^+) \zeta_{3,k} & i = 3 \\ -\beta_1(\tau_k^+) \rho_{3,k} & i = 4 \end{cases} \tag{31}$$

**Case (8b)** A NEP of queue 3 starts while  $z_3(\tau_k) = 0$ ,  $z_4(\tau_k) > 0$ . This may happen in two ways. First,  $\alpha_3(\tau_k)$  becomes positive because a  $R2G_1$  event occurs. Then (27) applies, where  $x'_{3,i}(\tau_k^-) = 0$ . Second,  $\beta_1(\tau_k)$  becomes positive because either  $h_1(\tau_k)$  or  $\alpha_1(\tau_k)$  switches from 0 to a strictly positive value, either being an exogenous event. Therefore,

$$x'_{3,i}(\tau_k^+) = x'_{3,i}(\tau_k^-) = 0, \quad i = 1, 2, 3, 4 \tag{32}$$

**Case (8c)** A NEP of queue 3 starts while  $z_4(\tau_k) = 0$ ,  $z_3(\tau_k) > 0$ . This may also happen in two ways. First,  $x_3(\tau_k^+)$  becomes positive because a  $R2G_1$  event occurs, which makes  $\alpha_3(t)$  larger. Then (27) applies, where  $x'_{3,i}(\tau_k^-) = 0$ . Second, it is due to a change of value in either  $h_1(\tau_k)$  or  $\alpha_1(\tau_k)$  or  $\beta_3(\tau_k)$ , which are all exogenous events. Therefore,  $x'_{3,i}(\tau_k^+)$  is the same as in (32).

- (9) **Event  $SF_3$  starts a FP of queue 3.** This is an endogenous event that occurs when  $g_k(x(\theta, t), \theta) = x_3(\theta, t) - s_3 = 0$ . Using (20), we get

$$\tau'_{k,i} = \frac{-x'_{3,i}(\tau_k^-)}{f_{3,k-1}(\tau_k^-)} \tag{33}$$

This event may happen either (i) when queue 3 has a RED light and queue 1 has a GREEN light, or (ii) both queues 1 and 3 have a GREEN light but the departure rate of queue 1 exceeds that of queue 3.

Looking at (7), in case (i),  $\dot{x}_3(t)$  switches from (7.1) to (7.6) or from (7.2) to (7.6). In case (ii), we have either  $h_1(t) > h_3(t)$  or  $\alpha_1(t) > h_3(t)$ , so that  $\dot{x}_3(t)$  switches either from (7.3) to (7.6) or from (7.4) to (7.6). In all such cases, we have  $f_{3,k}(\tau_k^+) = 0$ , hence  $f_{3,k-1}(\tau_k^-) - f_{3,k}(\tau_k^+) = f_{3,k-1}(\tau_k^-)$ . Combining this with (33), it follows from (19) that

$$x'_{3,i}(\tau_k^+) = 0, \quad i = 1, \dots, 4 \tag{34}$$

Observe that this event also affects the dynamics of queue 1 in (6) and queue 2 in (8) due to the presence of the condition  $x_3 = s_3$ , which was not encountered in our earlier work (Geng and Cassandras 2012a) where blocking was ignored. We first derive  $x'_{1,i}(\tau_k^+)$  as follows.

Looking at (6), let us consider once again cases (i) and (ii) above. In case (i), if  $x_1(t) > 0$ , then  $\dot{x}_1(t)$  switches from  $\alpha_1(t) - h_1(t)$  to  $\alpha_1(t)$  and we have:  $f_{1,k-1}(\tau_k^-) - f_{1,k}(\tau_k^+) = -h_1(t)$  and  $f_{3,k-1}(\tau_k^-) = h_1(t)$ . Thus, according to (19)  $x'_{1,i}(\tau_k^+) = x'_{1,i}(\tau_k^-) + x'_{3,i}(\tau_k^-)$ . Similarly, if  $x_1(t) = 0$ , then  $\dot{x}_1(t)$  switches from 0 to  $\alpha_1(t)$  and we have:  $f_{1,k-1}(\tau_k^-) - f_{1,k}(\tau_k^+) = -\alpha_1(t)$ , and  $f_{3,k-1}(\tau_k^-) = \alpha_1(t)$ , leading again to  $x'_{1,i}(\tau_k^+) = x'_{1,i}(\tau_k^-) + x'_{3,i}(\tau_k^-)$ . In case (ii), while  $x_1(t) > 0$ ,  $\dot{x}_1(t)$  switches from  $\alpha_1(t) - h_1(t)$  to  $\alpha_1(t) - h_3(t)$ , so that  $f_{1,k-1}(\tau_k^-) - f_{1,k}(\tau_k^+) = h_3(t) - h_1(t)$ , and  $f_{3,k-1}(\tau_k^-) = h_1(t) - h_3(t)$ . Thus, (19) gives  $x'_{1,i}(\tau_k^+) = x'_{1,i}(\tau_k^-) + x'_{3,i}(\tau_k^-)$ . Similarly, this equation also applies while  $x_1(t) = 0$ . To conclude, in all cases we have:

$$x'_{1,i}(\tau_k^+) = x'_{1,i}(\tau_k^-) + x'_{3,i}(\tau_k^-), \quad i = 1, \dots, 4$$

This is the dual of (22) where we can see, that  $x'_{1,i}(\tau_k^+)$  explicitly depends on  $x'_{3,i}(\tau_k^-)$ . In this case, a ‘‘perturbation’’ in the content of queue 3 ‘‘propagates’’ upstream to queue 1 whenever an FP at queue 3 takes place.

Similarly, we derive  $x'_{2,i}(\tau_k^+)$ . Since an  $SF_3$  event occurs only when queue 1 has a GREEN light, queue 2 must then have a RED light at  $\tau_k$ . Looking at (8),  $f_{2,k}(\tau_k^+) = f_{2,k-1}(\tau_k^-) = \alpha_2(\tau_k)$ . Thus  $x'_{2,i}(\tau_k)$  does not change:

$$x'_{2,i}(\tau_k^+) = x'_{2,i}(\tau_k^-), \quad i = 1, \dots, 4 \tag{35}$$

- (10) **Event  $EF_3$  ends a FP of queue 3.** Looking at the case in (7) where  $\dot{x}_3 = 0$  with  $x_3 = s_3$ , we can see that this event occurs because the inflow rate of queue 3,  $\beta_1$ , becomes lower than the outflow rate  $\beta_3$ . There are four possible cases to consider.

**Case (10a)** *FP ends when queue 3 has a RED light and a R2G<sub>3</sub> event occurs.* In this case, the departure rate at queue 3 switches from 0 to  $h_3 > 0$ . This is an endogenous event which was analyzed in Case (6). According to (34),  $x'_{3,i}(t)$  is reset to 0 when the FP starts. During the FP, we have  $x_3(t) = s_3$ , therefore  $x'_{3,i}(t) = 0$  holds during the whole FP and  $x'_{3,i}(\tau_k^-) = 0$ .

Thus, (28) becomes

$$x'_{3,i}(\tau_k^+) = \begin{cases} 0 & i = 1, 2 \\ h_3(\tau_k^+) \zeta_{3,k} & i = 3 \\ h_3(\tau_k^+) \rho_{3,k} & i = 4 \end{cases} \quad (36)$$

For queue 1, if  $G_1(\tau_k) = 1$ , we have  $f_{1,k-1}(\tau_k^-) = \alpha_1(\tau_k)$  because the departure process is blocked, and  $f_{1,k}(\tau_k^+) = \alpha_1(\tau_k) - h_1(\tau_k)$  because the queue 1 departure process is resumed and  $h_1(\tau_k) < h_3(\tau_k)$ . Hence we have  $f_{1,k-1}(\tau_k^-) - f_{1,k}(\tau_k^+) = h_1(\tau_k)$ . Based on Lemma 2, we have  $\tau'_{k,3} = \zeta_{3,k}$ ,  $\tau'_{k,4} = \rho_{3,k}$ ,  $\tau'_{k,1} = 0$  and  $\tau'_{k,2} = 0$ . Thus, according to (19) we get

$$x'_{1,i}(\tau_k^+) = x'_{1,i}(\tau_k^-) + \begin{cases} 0 & i = 1, 2 \\ h_1(\tau_k^+) \zeta_{3,k} & i = 3 \\ h_1(\tau_k^+) \rho_{3,k} & i = 4 \end{cases} \quad (37)$$

If, on the other hand,  $G_1(\tau_k) = 0$ , we have  $f_{1,k-1}(\tau_k^-) - f_{1,k}(\tau_k^+) = 0$ , so that

$$x'_{1,i}(\tau_k^+) = x'_{1,i}(\tau_k^-) \quad i = 1, 2, 3, 4 \quad (38)$$

Similarly, we derive  $x'_{2,i}(\tau_k^+)$ . If  $G_2(\tau_k) = 1$ , we have  $f_{2,k-1}(\tau_k^-) = \alpha_2(\tau_k)$  because the departure process is blocked, and  $f_{2,k}(\tau_k^+) = \alpha_2(\tau_k) - h_2(\tau_k)$  because the queue 2 departure process is resumed. Hence, we have  $f_{2,k-1}(\tau_k^-) - f_{2,k}(\tau_k^+) = h_2(\tau_k)$ . Therefore,

$$x'_{2,i}(\tau_k^+) = x'_{2,i}(\tau_k^-) + \begin{cases} 0 & i = 1, 2 \\ h_2(\tau_k^+) \zeta_{3,k} & i = 3 \\ h_2(\tau_k^+) \rho_{3,k} & i = 4 \end{cases} \quad (39)$$

If  $G_2(\tau_k) = 0$ ,  $x'_{2,i}(\tau_k)$  does not change and (35) applies.

**Case (10b)** *FP ends when both queues 1,3 have a GREEN light, and a G2R<sub>1</sub> event occurs.* In this case,  $\beta_1(t)$  decreases from a positive value to 0. This is an endogenous event which was analyzed in Case (3) and (24) applies for  $x'_{3,i}(\tau_k^+)$  where  $x'_{3,i}(\tau_k^-) = 0$  since,  $x_3(t) = s_3$  during the whole FP, therefore  $x'_{3,i}(t) = 0$ . For  $x'_{1,i}(\tau_k^+)$ , we have (see Geng and Cassandras 2012b):

$$x'_{1,i}(\tau_k^+) = \begin{cases} x'_{1,i}(\tau_k^-) - \beta_1(\tau_k^-) \zeta_{1,k} & i = 1 \\ x'_{1,i}(\tau_k^-) - \beta_1(\tau_k^-) \rho_{1,k} & i = 2 \\ x'_{1,i}(\tau_k^-) & i = 3, 4 \end{cases} \quad (40)$$

Similarly for  $x'_{2,i}(\tau_k^+)$ , we have  $f_{2,k-1}(\tau_k^-) - f_{2,k}(\tau_k^+) = \beta_2(\tau_k)$ , and

$$x'_{2,i}(\tau_k^+) = \begin{cases} x'_{2,i}(\tau_k^-) + \beta_2(\tau_k^+) \zeta_{1,k} & i = 1 \\ x'_{2,i}(\tau_k^-) + \beta_2(\tau_k^+) \rho_{1,k} & i = 2 \\ x'_{2,i}(\tau_k^-) & i = 3, 4 \end{cases} \quad (41)$$

**Case (10c)** *FP ends when both queues 1,3 have a GREEN light, and a E<sub>1</sub> event occurs.* In this case,  $\beta_1(t)$  decreases from  $h_1(t)$  to  $\alpha_1(t)$  or 0. This is also an endogenous event analyzed in Case (1) and (22) applies for  $x'_{3,i}(\tau_k^+)$

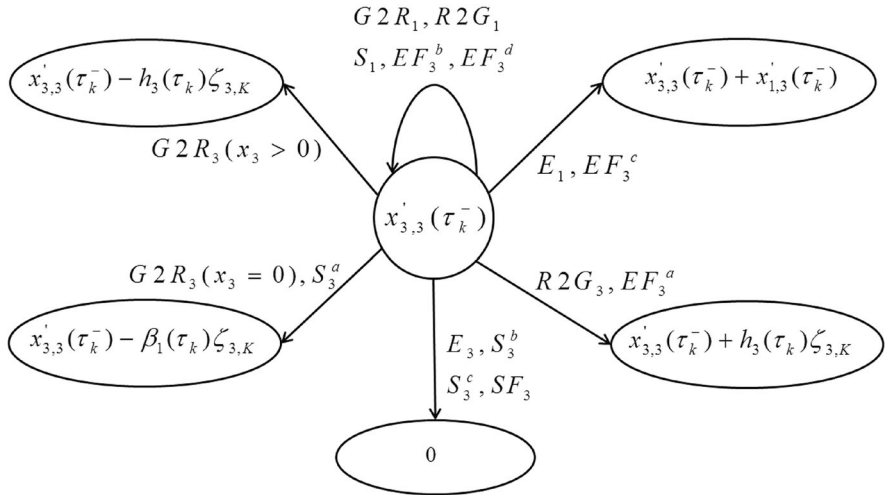


Fig. 6 Transition diagram summarizing  $x'_{3,3}$  updated after each event

where  $x'_{3,i}(\tau_k^-) = 0$ . For  $x'_{1,i}(\tau_k^+)$ , we have (see Geng and Cassandras 2012b):

$$x'_{1,i}(\tau_k^+) = 0, \quad i = 1, \dots, 4 \tag{42}$$

Finally, since  $E_1$  must occur while  $G_2(t) = 0$ , (35) applies for  $x'_{2,i}(\tau_k^+)$ .

**Case (10d)** *FP ends when both queues 1,3 have a GREEN light, and the sign of  $\beta_1(t) - h_3(t)$  randomly switches from non-negative to strictly negative.* This occurs because either  $h_3(t)$  increases or  $\beta_1(t)$  decreases. In the former case,  $h_3(t)$  increasing is obviously an exogenous event, hence  $\tau'_{k,i} = 0$ . What causes  $\beta_1(t)$  to decrease could also be an exogenous event, e.g., either  $\alpha_1(t)$  or  $h_1(t)$  randomly decreases in (3). In this case, it follows from (19) that

$$x'_{3,i}(\tau_k^+) = x'_{3,i}(\tau_k^-) \quad i = 1, 2, 3, 4 \tag{43}$$

$$x'_{1,i}(\tau_k^+) = x'_{1,i}(\tau_k^-) \quad i = 1, 2, 3, 4 \tag{44}$$

$$x'_{2,i}(\tau_k^+) = x'_{2,i}(\tau_k^-) \quad i = 1, 2, 3, 4 \tag{45}$$

This completes the derivation of all state and event time derivatives required to evaluate the sample performance derivative in (17). Figure 6 is used to illustrate all transitions involved in the evaluation of  $x'_{3,3}$  after each event, using the notation  $S_3^a$  to represent event  $S_3$  corresponding to case  $a$  in (31) as opposed to cases  $b, c$  in (32). Similar notation applies for  $S_3^b, S_3^c, EF_3^a, EF_3^b, EF_3^c, EF_3^d$ . Similar transition diagrams can be used to summarize the evaluation of all other state derivations based on the above results (22)–(45). It is worth pointing out in Fig. 6 that there is only one case where  $x'_{3,3}$  is coupled to another state derivatives: when  $E_1$  or  $EF_3^c$  occurs.

Using the definition of  $L_{n,m}(\theta)$  in (13), note that we can decompose (17) into its NEPs and evaluate the derivatives  $dL_{n,m}(\theta)/d\theta_i$  as shown next.

### 3.3 Cost derivative

By virtue of (21),  $x'_{n,i}(t)$  is piecewise constant during a NEP and its value changes only at an event point  $t_{n,m}^j$ ,  $j = 1, \dots, J_{n,m}$ . Therefore, we have

$$\begin{aligned} \frac{dL_{n,m}(\theta)}{d\theta_i} &= x'_{n,i}(\xi_{n,m}^+) (t_{n,m}^1 - \xi_{n,m}) + x'_{n,i}((t_{n,m}^{J_{n,m}})^+) (\eta_{n,m} - t_{n,m}^{J_{n,m}}) \\ &\quad + \sum_{j=2}^{J_{n,m}} x'_{n,i}((t_{n,m}^j)^+) (t_{n,m}^j - t_{n,m}^{j-1}) \end{aligned}$$

Clearly,  $x'_{n,i}$  at each event point is determined by (19) which in turn depends on the event type at  $t_{n,m}^j$ ,  $j = 1, \dots, J_{n,m}$  and is given by the corresponding expression in (22) through (45). An explicit closed-form expression of  $dL_{n,m}(\theta)/d\theta_i$  may be obtained in this manner but becomes complicated. However, an algorithm that updates  $dL_{n,m}(\theta)/d\theta_i$  after every observed event is simple to implement.

More importantly, note that this IPA derivative depends on the following information:

- i) the number of events in each NEP  $J_{n,m}$
- ii) the number of total  $G2R_n$  events  $\zeta_{n,k}$
- iii) the number of total  $R2G_n$  events  $\rho_{n,k}$
- iv) the event times  $\xi_{n,m}$ ,  $\eta_{n,m}$  and  $t_{n,m}^j$
- v) the arrival and departure rates  $\alpha_n(\tau_k)$ ,  $\beta_n(\tau_k)$  at  $G2R_n$  and  $R2G_n$  event times *only*.

The quantities in (i) – (iv) are easily observed through counters and timers. The rates in (v) may be obtained through simple rate estimators. We emphasize that they are *only* needed at  $G2R_n$  and  $R2G_n$  event times, which are deterministic and pre-determined once the control parameter  $\theta$  is chosen.

It is important to point out that IPA is an event-driven method, scalable in the number of observed events over a sample path. Moreover, each step of an IPA estimator processes a specific event in the event set, so that many of the observed events trigger the same form of computation. As the complexity of a system grows in the number of states, the cardinality

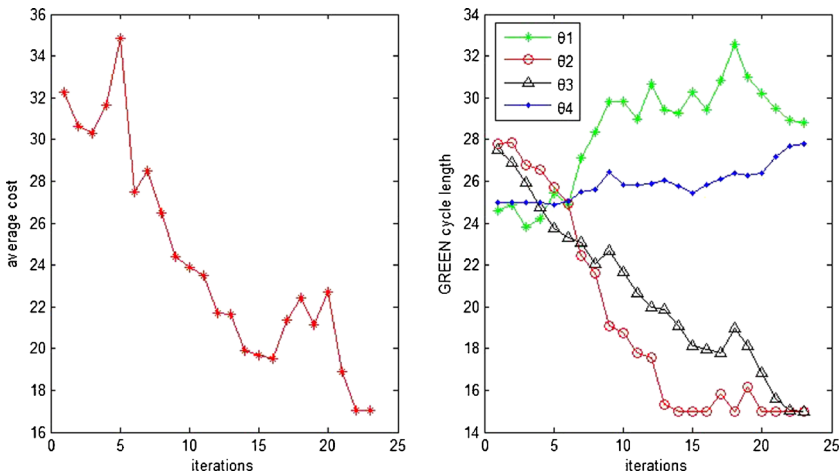


Fig. 7 Sample trajectories of  $J$  and  $\theta$  using IPA

**Table 1** IPA vs BF method  
 results:  $s_3 = 1000$ ,  
 $1/\alpha = [4, 4, 4]$

w	BF		IPA	
	$\theta^*$	$J^*$	$\theta^*$	$J^*$
[1,1,1,1]	[15,15,15,15]	5.4	[15,15,15,15]	5.4
[10,1,1,1]	[27,15,15,29]	16.6	[28.8,15,15,27.8]	17.5
[1,5,5,1]	[15,23,17,21]	12.6	[15.1,18.6,15.6,18.5]	13.2
[5,1,1,10]	[25,15,15,25]	22.0	[22.1,15,15,22.9]	22.5
[1,10,1,1]	[15,29,15,29]	16.3	[15, 31.2,18.1,26.6]	17.2

of the event set generally grows at a much lower rate and, on occasion, may not even change since new state transitions may be caused by the same types of events already included in the event set  $\Phi_n$ . Thus, even though the complexity of the hybrid automata shown in Figs. 2 and 3 may rapidly increase with the number of traffic flows and intersections, the IPA estimator depends only on the events causing state transitions and not the states themselves.

### 4 Simulation examples

In this section, we describe how the IPA estimators derived for the SFM can be used to determine optimal light cycles for two intersections modeled as a DES. We apply the IPA estimators using actual data from an observed sample path of the system (in this case, by simulating it as a pure DES).

We assume cars arrive according to a Poisson process with rate  $\bar{\alpha}_n, n = 1, 2, 4$  (as already emphasized, our results are independent of this distribution.). We also assume cars depart at a rate  $h_n(t)$  which we fix to be a constant  $H_n$  when the road is not empty. We also constrain  $\theta_i, i = 1, \dots, 4$ , to take values in an interval  $[\theta_{\min}, \theta_{\max}]$ .

For the simulated DES model, we use a brute-force (BF) method to find an optimal  $\theta_{BF}^*$ : we discretize all real values of  $\theta_i$  and for  $\theta_i, i = 1, \dots, 4$  combinations we run 10 sample paths to obtain the average total cost. The value of  $\theta_{BF}^*$  is the one generating the least average cost, to be compared to  $\theta_{IPA}^*$ , the IPA-based method where a standard gradient-based iteration in  $\theta$  is used. In our simulations, we estimate  $\alpha_n(\tau_k)$  at an event time  $\tau_k$  through  $N_a/t_w$  by counting car arrivals  $N_a$  over a time window  $t_w$  around  $\tau_k: [\tau_k - t_w/2, \tau_k + t_w/2]$ .

In our first example, we set  $\bar{\alpha}_n = 1/4, n = 1, 2, 4, H_n = 1, n = 1, \dots, 4, \theta_{\min} = 15sec, \theta_{\max} = 40sec, T = 1000sec$ , initial queue content  $X_0 = [5, 1, 5, 1]$  and initial GREEN light starting at queue 1 and 3, i.e.,  $z_1(0) = z_3(0) = 0$  and  $\dot{z}_1(0) = \dot{z}_3(0) = 1$ . We first

**Table 2** IPA vs BF method  
 results:  $s_3 = 10, 1/\alpha = [4, 4, 4]$

w	BF		IPA	
	$\theta^*$	$J^*$	$\theta^*$	$J^*$
[1,1,1,1]	[15,15,15,15]	5.5	[15,15,15,15]	5.5
[10,1,1,1]	[29,15,24,15]	18.5	[27.3,15,25.5,15]	17.7
[1,5,5,1]	[15,23,17,21]	13.3	[15,20.2,15,21.6]	13.6
[5,1,1,10]	[21,15,15,31]	24.8	[23.2,15,15,32.1]	22.9
[1,10,1,1]	[15,29,15,29]	17.0	[15, 31.2,15,28.7]	17.3

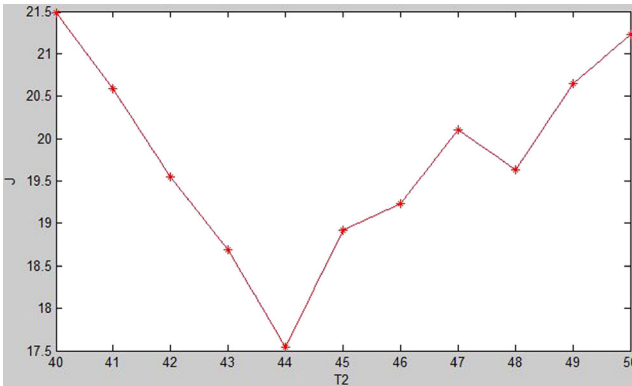


**Fig. 8**  $J_{IPA}^*$  at different red + green cycle length  $T_2$

set  $s_3 = 1000$ , which is long enough to avoid blocking. Figure 7 shows typical sample trajectories of  $J$  and  $\theta$  using the IPA-based method where  $w = [10, 1, 1, 1]$  and initial  $\theta_0 = [25, 30, 30, 25]$ . The light cycles are adjusted after every iteration whose duration is  $T$ . More results are shown in Table 1. We then set the capacity of queue 3 at  $s_3 = 10$ . Simulation results in this case are shown in Table 2 using the same settings. As we can see,  $\theta_{IPA}^*$  is numerically close to the best values obtained by the BF method. Note that the BF method becomes impractical when the number of controllable parameters or their range is large. However, the IPA method is scalable and still effective in such situations. In addition, we observe that the optimal cost obtained in all cases in Table 2 is slightly larger compared to Table 1, which is due to the blocking effect at queue 3, as expected.

An interesting observation is that the value of  $(\theta_3 + \theta_4) \equiv T_1$  is approaching that of  $(\theta_1 + \theta_2) \equiv T_2$  if  $T$  is sufficiently large. This indicates that the two intersections tend to have the same traffic light switching cycle to balance traffic flows. For example, in Fig. 8, we set  $w = [1, 10, 1, 1]$  and change  $T_2$  to obtain  $J_{IPA}^*$  while keeping  $T_1 = 44$ . As we can see, the minimum  $J_{IPA}^*$  is achieved when  $T_1 = T_2$ , which also matches the observations under independent  $\theta_i$ .

Based on this observation, we carry out additional simulation examples by setting the “GREEN plus RED” cycle to a fixed value for each intersection. With this constraint, we only need to find optimal  $\theta_1^*$  and  $\theta_3^*$ , since  $\theta_2^* = T_1 - \theta_1^*$  and  $\theta_4^* = T_2 - \theta_3^*$ . We let  $T_1 = T_2 = 40$ , which restricts the two intersections to have the same traffic light switching cycle. Table 3 shows the simulation results obtained under different traffic intensities, with  $w = [1, 1, 1, 1]$  and  $T = 3000$ . We make the following observations: (1) if queue 1 has a larger

**Table 3** IPA vs BF method under different traffic intensities

$1/\alpha$	BF		IPA	
	$[\theta_1^*, \theta_3^*]$	$J^*$	$[\theta_1^*, \theta_3^*]$	$J^*$
[2,2,3]	[19, 23]	72.8	[19.9, 20.0]	56.9
[2,3,3]	[23, 23]	18.5	[22.5, 23.0]	16.1
[3,3,2]	[17, 17]	15.9	[17.5, 17.0]	14.5
[4,4,3]	[15, 15]	7.1	[16.1, 15.8]	7.1
[3,3,5]	[21, 21]	8.9	[19.0, 19.6]	8.5

**Table 4** IPA vs BF method under different  $X_0$

$X_0$	$1/\alpha$	BF		IPA	
		$[\theta_1^*, \theta_3^*]$	$J^*$	$[\theta_1^*, \theta_3^*]$	$J^*$
[8,1,8,1]	[1.5,3,2]	[21,21]	229	[25.9,25.5]	207
[8,1,3,1]	[1.5,3,2]	[22,21]	222	[25.4,25.2]	199
[3,1,8,1]	[1.5,3,2]	[21,22]	223	[24.4,24.1]	197
[100,1,3,1]	[1.5,3,2]	[23,23]	312	[24.7,24.2]	293
[100,1,2,1]	[5,3,2]	[17,17]	23.3	[16.1,17.5]	22.0

incoming traffic rate than queue 4, then queue 3 has a longer GREEN cycle than queue 4; (2) if queue 4 has a larger incoming traffic rate than queue 1, then queue 2 has a longer GREEN cycle than queue 1 even if they have the same arrival rate. All these observations are reasonable because the optimal traffic light settings seek to coordinate two intersections to avoid traffic blocking.

We are also interested to see the optimal control parameters under different initial traffic conditions, as shown in Table 4. Clearly  $\theta^*$  depends on the initial queue content. An interesting case is when  $X_0 = [100, 1, 2, 1]$ . Even though there is high traffic at queue 1 initially, the future incoming traffic flow is relatively low. Thus the GREEN cycle at queue 1 is still less than queue 2 over  $T = 3000$ .

Figure 9 shows the optimal cost and GREEN cycle length when the capacity of queue 3 varies, where we set  $1/\alpha = [2, 3, 2]$  and initial GREEN light at queue 1 and 4, i.e.,  $z_1(0) = z_4(0) = 0$  and  $\dot{z}_1(0) = \dot{z}_4(0) = 1$ . Now the GREEN light starting times of queue 1 and queue 3 do not match, thus more blocking events may occur; this suggest that such traffic light offset is another controllable parameter which may be used to improve performance. As we can see, there is less blocking (less cost) with larger queue 3 capacity.

It must be pointed out that the BF method does not provide a “true” optimal, since the DES model of the traffic system is as much an approximation as the SFM based on which IPA operates. Thus, the comparative results should be interpreted accordingly.

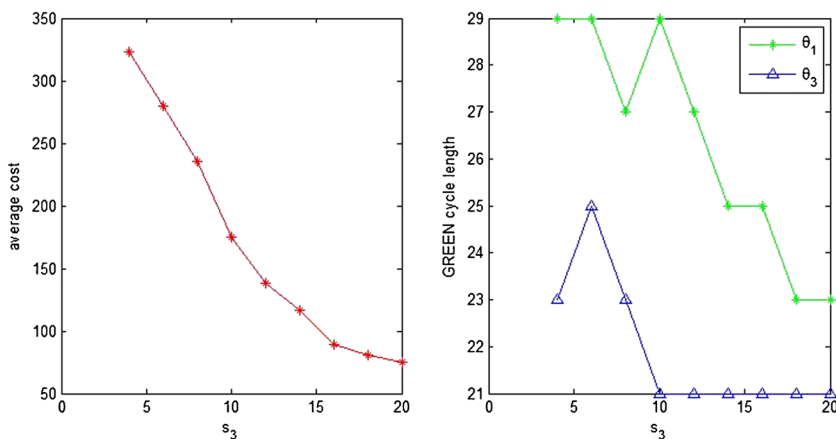


**Fig. 9** Optimal parameters at different  $s_3$

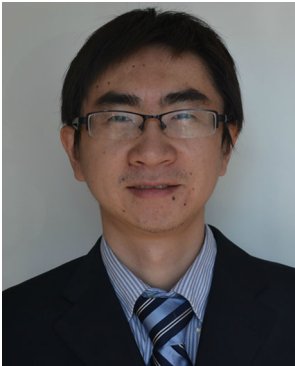
## 5 Conclusion

We have developed a SFM for a traffic light control problem with two coupled intersections, based on which we derive an IPA gradient estimator of a cost metric with respect to the green and red cycle lengths. The estimators are used to iteratively adjust light cycle lengths to improve performance and, under proper conditions, obtain optimal values. The analysis in the paper can be readily extended to  $N$  intersections in tandem. We also observe that in the model presented here, we assume there is no travelling delay between two intersections, i.e.,  $\alpha_3(t) = \beta_1(t)$ , which is not realistic especially if road 3 is very long. Future work will consider a delay  $\Delta t(x)$  so that  $\alpha_3(t) = \beta_1(t - \Delta t(x))$ , where  $\Delta t(x)$  generally depends on the content of queue 3. It is also worth incorporating more accurate dynamics for departure processes  $h_n(t)$ ; this involves the accelerating rate right after a  $R2G$  event and a decelerating rate right before a  $G2R$  event. Moreover,  $h_n(t)$  should also depend on the content of the associated downstream queue. Other future work includes controlling the offset of traffic light cycles (in addition to cycle length), adding left and right turn traffic, and extending the analysis to multiple junctions in a road network.

## References

- Abdulhai B, Pringle R, Karakoulas G (2003) Reinforcement learning for true adaptive traffic signal control. *J Transp Eng* 129(3):278–285
- Alvarez I, Poznyak A (2010) Game theory applied to urban traffic control problem. In: International conference on control, automation and systems, pp 2164–2169
- Bazzan AL (2009) Opportunities for multiagent systems and multiagent reinforcement learning in traffic control. *Auton Agent Multi-Agent Syst* 18:342–375
- Cassandras CG, Lafortune S (2008) Introduction to Discrete Event Systems, 2nd edn. Springer, Berlin
- Cassandras CG, Lygeros J (2006) Stochastic hybrid systems. Taylor and Francis, New York
- Cassandras CG, Wardi Y, Melamed B, Sun G, Panayiotou CG (2002) Perturbation analysis for on-line control and optimization of stochastic fluid models. *IEEE Trans Automat Control* 47(8):1234–1248
- Cassandras CG, Wardi Y, Panayiotou CG, Yao C (2010) Perturbation analysis and optimization of stochastic hybrid systems. *Eur J Control* 16(6):642–664
- DeSchutter B (1999) Optimal traffic light control for a single intersection. *Proc IEEE Am Control Conf* 3:2195–2199
- Dong C (2004) Area traffic signal timing optimization based on chaotic and genetic algorithm approach. *Comput Eng Appl* 40(29):32–34
- Dong C (2006) Chaos-particle swarm optimization algorithm and its application to urban traffic control. *Int J Comput Sci Netw Secur* 6(1):97–101
- Dujardin Y, Boillot F, Vanderpooten D, Vinant P (2011) Multiobjective and multimodal adaptive traffic light control on single junctions. In: 14th IEEE conference on intelligent transportation systems, pp 1361–1368
- Findler N, Stapp J (1992) A distributed approach to optimized control of street traffic signals. *J Transp Eng* 118
- Gartner NH (1983) OPAC: a demand-responsive strategy for traffic signal control. *Transp Res Rec* 906:75–81
- Geng Y, Cassandras CG (2012a) Multi-intersection traffic light control using infinitesimal perturbation analysis. In: 11th international workshop on discrete event systems, pp 104–109
- Geng Y, Cassandras CG (2012b) Traffic light control using infinitesimal perturbation analysis. In: 51st IEEE conference on decision and control, pp 7001–7006
- Head L, Ciarallo F, Kaduwela V, Lucas D (1996) A perturbation analysis approach to traffic signal optimization. In: INFORMS National Meeting
- Henry JJ, Farges JL (1990) PROLYN control, computers, communications in transportation. Pergamon Press, New York, pp 253–255
- Hunt PB, Robertson DL, Bretherton RD (1982) The SCOOT on-line traffic signal optimization technique. *Traffic Eng Control* 23:190–192

- Lee JH, Lee K, Lee-Kwang H (1995) Fuzzy controller for intersection group. In: International IEEE/IAS conference on industrial automation and control, pp 376–382
- Liu Q, Lu H, Zou B, Li Q (2006) Design and development of parking guidance information system based on web and gis technology. In: 6th international conference on ITS telecommunications, pp 1263–1266
- Lowrie PR (1982) SCATS principles, methodology, algorithm. In: IEE conference on road traffic signalling, pp 67–70
- Murat YS, Gedizlioglu E (2005) A fuzzy logic multi-phased signal control model for isolated junctions. *Transp Res Part C* 18:19–36
- Nakatsuyama M, Nagahashi H, Nishizuka N (1984) Fuzzy logic phase controller for traffic junctions in the one-way arterial road. In: IFAC 9th triennial world cong, pp 2865–2870
- Niittymaki J, Nevala R, Turunen E (2002) Fuzzy traffic signal control and a new interface method-maximal fuzzy similarity. In: Proceedings of the 13th Mini-EURO Conference, pp 716–728
- Panayiotou CG, Howell WC, Fu M (2005) Online traffic light control through gradient estimation using stochastic fluid models. In: Proceedings of the IFAC 16th triennial world congress
- Papageorgiou M, Diakaki C, Dinopoulou V, Kotsialos A, Wang Y (2003) Review of road traffic control strategies. *Proc IEEE* 91(12):2043–2067
- Pappis C, Mamdani E (1977) A fuzzy logic controller for a traffic junction. *IEEE Trans Syst Man Cybern SMC-7* 7(10):707–717
- Porche I, Lafortune S (1999) Adaptive look-ahead optimization of traffic signals. *ITS J* 4:209–254
- Prashanth LA, Bhatnagar S (2011) Reinforcement learning with function approximation for traffic signal control. *IEEE Trans Intell Transp Syst* 12(2):412–421
- Robertson DI, Bretherton RD (1991) Optimizing networks of traffic signals in real-time: the SCOOT method. *IEEE Trans Veh Technol* 40(1):11–15
- Sen S, Head L (1997) Controlled optimization of phases at an intersection. *Transp Sci* 31:5–17
- Thorpe T (1997) Vehicle traffic light control using sarsa. Master thesis, Department of Computer Science, Colorado State Univ
- Trabia MB, Kaseko MS, Ande M (1996) A two-stage fuzzy logic controller for traffic signals. *Transp Res Part C* 7(6):353–367
- Wardi Y, Adams R, Melamed B (2010) A unified approach to infinitesimal perturbation analysis in stochastic flow models: the single-stage case. *IEEE Trans Automat Control* 55(1):89–103
- Wei W, Zhang Y, Mbede JB, Zhang Z, Song J (2001) Traffic signal control using fuzzy logic and MOGA. In: IEEE international conference on systems, man, and cybernetics, pp 1335–1340
- Wen Y, Wu T (2005) Reduced-order rolling horizon optimization of traffic control based on ant algorithm. *J Zhejiang Univ (Med Sci)* 39(6):835–839
- Wiering M, Veenen J, Vreeken J, Koopman A (2004) Intelligent traffic light control. Technical Report UU-CS-2004
- Yao C, Cassandras CG (2011) Resource contention games in multiclass stochastic flow models. *Nonlinear Anal Hybrid Syst* 5(2):301–319
- Yu X, Recker W (2006) Stochastic adaptive control model for traffic signal systems. *Transp Res Part C Emerg Technol* 14(4):263–282
- Zhao X, Chen Y (2003) Traffic light control method for a single intersection based on hybrid systems. In: Proceedings of the IEEE intelligent transp. systems, pp 1105–1109



**Yanfeng Geng** received his PhD degree from Division of Systems Engineering of Boston University in 2013 and B.S. degree from University of Science and Technology of China in 2005. His research interests focus on Intelligent Transportation System, Optimal Control and Stochastic Optimization. He is a student member of IEEE. He is now working at Amazon.



**Christos G. Cassandras** is Head of the Division of Systems Engineering and Professor of Electrical and Computer Engineering at Boston University. He received degrees from Yale University, Stanford University, and Harvard University. He specializes in discrete event and hybrid systems, stochastic optimization, and computer simulation, with applications to computer and sensor networks, manufacturing, and transportation systems. He has published over 300 refereed papers in these areas, and five books. He has collaborated with The MathWorks, Inc. in the development of the discrete event and hybrid system simulator SimEvents. Dr. Cassandras was Editor-in-Chief of the *IEEE Transactions on Automatic Control* (1998–2009) and 2012 President of the IEEE Control Systems Society. He has been a plenary speaker at many international conferences and the recipient of several awards, including the 2011 IEEE Control Systems Technology Award, the Distinguished Member Award of the IEEE Control Systems Society (2006), the 1999 Harold Chestnut Prize, a 2011 prize for the IBM/IEEE Smarter Planet Challenge competition, a 1991 Lilly Fellowship and a 2012 Kern Fellowship. He is a member of Phi Beta Kappa and Tau Beta Pi and a Fellow of the IEEE and the IFAC.